Journal of Materials Chemistry A

Co-N4 Moiety Embedded into Graphene as an Efficient Single-Atom-Catalyst for NO Electrochemical Reduction: a Computational Study

Journal:	*Journal of Materials Chemistry A*
Manuscript ID	TA-ART-01-2018-000875.R1
Article Type:	Paper
Date Submitted by the Author:	15-Mar-2018
Complete List of Authors:	Wang, Zhongxu; Harbin Normal University, Chemistry Zhao, Jing-Xiang; Harbin Normal University, Chemistry Wang, Jingyang; Institute of Metal Research, High-Performance Ceramics Division Cabrera, Carlos; University of Puerto Rico, Department of Chemistry Chen, Zhongfang; University of Puerto Rico, Department of Chemistry

Co-N_4 Moiety Embedded into Graphene as an Efficient Single-Atom-Catalyst for NO Electrochemical Reduction: a Computational Study

Zhongxu Wang,[†] Jingxiang Zhao,[*,†] Jingyang Wang,[‡]

Carlos R. Cabrera,[#] Zhongfang Chen[*,#]

[†] College of Chemistry and Chemical Engineering, and Key Laboratory of Photonic and Electronic Bandgap Materials, Ministry of Education, Harbin Normal University, Harbin, 150025, China

[‡] Shenyang National Laboratory for Materials Science, Institute of Metal Research, Chinese Academy of Sciences, Shenyang 110016, China

[#] Department of Chemistry, University of Puerto Rico, Rio Piedras Campus, San Juan, PR 00931, USA

[*] To whom correspondence should be addressed. Email: xjz_hmily@163.com (JZ) ; zhongfangchen@gmail.com (ZC)

ABSTRACT: Electrochemical reduction of nitric oxide (NOER) is a promising technology for the removal of harmful N-containing species in groundwater under mild conditions. In this work, by means of density functional theory computations, we systematically investigated the potential of utilizing the experimentally feasible transition metal-N_4/graphenes as the NOER catalysts. Our results revealed that NO molecule can be moderately activated on the Co-N_4 moiety embedded into graphene, and the subsequent NOER steps can proceed to form either NH_3 at low coverages or N_2O at higher coverages. Especially, the computed onset potential of NOER on the Co-N_4/graphene (ca. -0.12 V) is comparable to (even better than) those on the well-established Pt-based catalysts. Thus, Co-N_4/graphene is a promising single-atom-catalyst with high efficiency for NO electrochemical reduction, which opens a new avenue of NO reduction for the environmental concerns.

1. INTRODUCTION

Nitrogen is the next most abundant element in the human body after carbon, hydrogen, and oxygen, and its conversion within the nitrogen cycle can produce a variety of inorganic compounds, including ammonia (NH_3), nitrite (NO_2^-), nitrate (NO_3^-), nitric oxide (NO), nitrous oxide (N_2O), and so on.[1, 2] Among these compounds, ammonia is crucial to sustain all forms of life because all organisms use it as one of the starting building blocks for the synthesis of amino acids, nucleotides, and many other important biological compounds, and ammonium nitrate has been commonly used as an explosive or in agriculture as a nitrogen-rich fertilizer.[3] However, the over-fertilization has led to the high concentrations of nitrate and nitrite ions in groundwater,[2-4] which are one of the main sources of pollution in groundwater and pose a serious threat to human health, such as methemoglobinemia and cancer.[4] Therefore, groundwater remediation for nitrate has become a topic of great environmental concern.[3]

Electrochemical denitrification offers a promising technology to remove nitrate from groundwater, and is considered as a plausible alternative for overcoming the limitations of biological denitrification and catalytic hydrogenation processes due to its high-efficiency, low-costs, environmental compatibility, and safety.[3-19] Various products, such as NO, N_2O, NH_3OH^+, and NH_4^+, can be produced during nitrate and nitrite electroreduction,[20, 21] and NO is proposed to be a key intermediate species that can determine product selectivity and affect the overall reaction rate.[3, 4] Additionally, NO emission control is also an important issue within the nitrogen cycle. Thus, the investigation on NO electrochemical reduction (NOER) is an essential step not only to

understand the fundamentals of NO_2^-/NO_3^- electrochemistry, but also to facilitate developing novel and effective electrochemical denitrification catalysts.[22-27]

To date, platinum (Pt) has been widely employed as the electrocatalyst for NO electrochemical reduction[13, 16, 18, 28-40] through two different ways: reductive stripping of strongly surface bonded NO in the absence of NO in solution, and continuous NO reduction in the presence of NO in solution.[3] For the former case, ammonia can be yielded at modest coverages (<0.45 ML; ML=monolayer) and relatively low potentials (< 0.4 V_{SHE}), in which HNO and NOH intermediate species are revealed to be key intermediates.[16] Under the continuous NO reduction, however, the main product is N_2O at potentials higher than 0.4 V_{SHE}.[40] In spite of the outstanding catalytic activity of Pt-based catalysts for NOER, their large-scale applications are greatly hampered by their high cost, limited supply, and poor durability. Thus, the search for alternative NOER catalysts with reduced amount of Pt or non-Pt remains a challenging but highly rewarding task.

The deposition of metal nanoclusters on substrates as heterogeneous catalysts has been confirmed to be quite promising alternative non-Pt catalysts.[41-43] The single-atom catalyst (SAC) is the ultimate small-size limit for metal nanoparticles, and its dispersion on substrates not only minimizes the usage of noble metal atoms to meet the ultimate goal of inexpensive catalysis, but also offers great potentials for achieving high activity and selectivity for many important electrochemical reactions,[44-52] such as nitrogen fixation,[48] oxygen reduction reaction,[46] and hydrogen production.[49]

Recent studies have demonstrated that the experimentally available transition metal (TM)/N/C material, which usually derives from the pyrolysis of metal complexes with macrocyclic N_4 ligands, is a promising stable, highly efficient, and low-cost catalyst for replacing Pt-based material for electrochemical reactions.[43-61] For example, Lin *et al.* reported a facile and effective strategy for the synthesis of Fe/N/C electrocatalysts and demonstrated their high catalytic activity for the oxygen reduction reaction (ORR) in both acidic and alkaline solutions.[56] Zhao *et al.* fabricated the single-atom dispersed Ni-N_4/C catalyst which possesses excellent performance for CO_2 electroduction.[59] Fei *et al.* successfully dispersed atomic Co on nitrogen-doped graphene, which is robust and highly active for hydrogen production in aqueous media with very low overpotentials (30 mV).[61] Li *et al.'s* DFT studies proposed that FeN_3-embedded graphene exhibits superior catalytic activity for the conversion of N_2 to NH_3 due to its high-spin polarization.[60]

The wide application of TM/N/C-based catalysts in electrochemical reactions inspires us to ask an interesting question: can they be utilized as good catalysts for NOER? To the best of our knowledge, there is no prior theoretical or experimental study on this appealing issue. Here, by means of comprehensive density functional theory (DFT) computations, we extensively explored the potential of a series of single TM atoms (Sc~Cu, Mo, Ru, and Rh) embedded into porphyrin-like graphene as the NOER electrocatalysts. Our results revealed that Co-N_4 moiety embedded into graphene exhibits excellent activity for the NOER, ammonia is the main product at low coverages through the HNO and HNOH species, while N_2O can be formed at

high coverages. Remarkably, the onset potential of the NOER on Co-N_4/graphene (ca. -0.12 V) is comparable to (even better than) those of Pt-based catalysts. Hence, the Co-N_4 moiety embedded into graphene is a quite promising single-atom catalyst for the electrochemical reduction of NO.

2. MODELS AND METHODS

Our spin-polarized DFT computations were performed by using the DMol^3 code.[62,63] The exchang-correlation interactions were treated by the Perdew-Burke-Ernzerhof (PBE) functional[64] within a generalized gradient approximation (GGA). The empirical correction in Grimme scheme[65] was applied to describe the van der Waals interactions between various intermediates and electrocatalysts. The density functional semi-core pseudopotential (DSPP) was utilized to consider for the relativistic effects of transition metals,[66] in which the core electrons are replaced by a single effective potential and some degree of relativistic corrections, while the double numerical plus polarization (DNP) basis set was used for other elements, whose accuracy can be comparable to that of Pople's 6-31G** basis set.[67] Self-consistent field (SCF) computations were performed with a convergence criterion of 10^{-6} a.u. on the total energy.

The single-atom catalysts were modeled by depositing one metal atom on a 5 × 5 supercell porphyrin-like graphene (containing 44 carbon and 4 nitrogen atoms), which was built by removing one C-C bond and replacing the four C atoms around the divacancy with four N atoms. The LST/QST tools in DMol^3 code were used to

locate the saddle points and minimum-energy pathways for N-O bond dissociation and protonation of intermediates species.[68] The Brillioun zone was sampled with a Monkhorst-Pack mesh with a 5 × 5 × 1 grid in reciprocal space during geometry optimization and transition state searching. The Hirshfeld population analysis was performed to compute the charge transfer. [69]

According to previous theoretical studies,[19, 28, 29] the NO electrochemical reduction proceeds via a series of net coupled proton and electron transfer (CPET), in which the main products are NH_3/NH_4^+, N_2, and N_2O. Each CPET step involves the transfer of a proton coupled with an electron from solution to an adsorbed species on the surface of catalyst. Thus, we computed the Gibbs free energy change (ΔG) of every elemental step using the standard hydrogen electrode model,[70-72] in which the chemical potential of $(H^+ + e^-)$ at pH = 0 is related to the chemical potential of 1 bar H_2 in the gas phase at 298 K. According to this method, the ΔG value can be determined: $\Delta G = \Delta E + \Delta ZPE - T\Delta S + \Delta G_U$,[73-75] where ΔE is the electronic energy difference directly obtained from DFT calculations. For example, the ΔE of NO adsorption on catalyst was defined as: $\Delta E = E_{NO/catalyst} - E_{NO} - E_{catalyst}$, where $E_{NO/catalyst}$, E_{NO}, and $E_{catalyst}$ are the DFT total energies for the NO adsorbed catalyst, free NO, and catalyst, respectively. ΔZPE is the change in zero-point energies, and TΔS is the entropy change at 298.15 K. ΔG_U is the free energy contributions related to electrode potential U. The zero–point energies and entropies of the NOER species were computed from the vibrational frequencies, in which only the adsorbate vibrational modes were computed explicitly, while the catalyst was fixed. The

entropies of the free molecules (NO, H_2, N_2O, NH_3) were taken from the standard thermodynamic database. The conductor-like screening model (COSMO) in DMol[3] was used with the dielectric constant of 78.54 to simulate the H_2O solvent environment.[76]

3. RESULTS AND DISSUCION

3.1. Screening NOER Catalyst Candidates.

The NO adsorption on the catalyst surface is the first step to initialize the NOER.[19, 28, 29] For an eligible electrocatalyst for NOER: 1) it should facilitate the chemisorption of NO to guarantee the sufficient activation of its N-O bond; 2) the ΔG value of NO on an ideal NOER catalyst should be as small as possible but large enough to prevent NO from desorbing from the catalyst surface according to the Sabatier principle.[77]

According to the above two criteria, we screened a series of single TM atoms, including Sc~Cu, Mo, Rh, and Ru, anchored on porphyrin-like N-doped graphene (namely, TM-N_4/graphene). To examine the adsorption strength of NO molecule on these materials, we computed the corresponding free energies, in which two different initial adsorption configurations were considered, namely end-on and side-on configurations.

Our DFT calculations showed that NO prefers to bind with the central TM atom via end-on configuration, leading to the formation of TM-N bond (Fig. 1a). The Ni-N_4/ and Cu-N_4/graphenes have positive ΔG values (Fig. 1b). According to

Criterion 1, these two materials are not appropriate as the NOER electrocatalysts. Following Criteria 2, the Co-N_4/graphene is expected to be the most eligible candidate for the NOER catalyst due to its moderate interaction strength with NO, while other catalysts exhibit too strong adsorption for NO. Thus, in the following sections, we will mainly focus on the NOER occurring on Co-N_4/graphene.

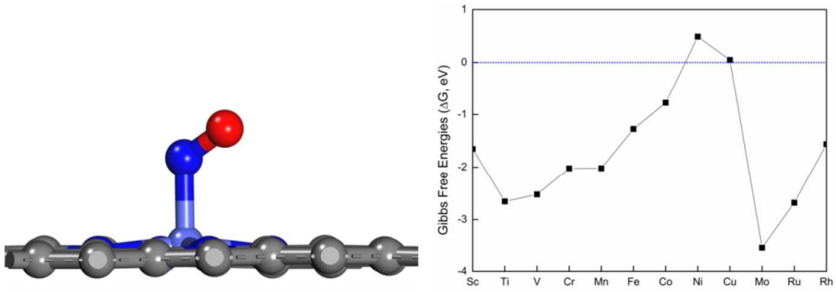

Fig. 1. (a) The schematic representation of the optimized structure of NO adsorbed on the TM-N_4/graphene, and (b) the corresponding Gibbs free energies at pH=0 and zero electrode potential.

3.2. NO adsorption on Co-N_4/graphene with different coverages

It is known that the products of NO electrochemical reduction reaction are highly dependent on the coverages of NO: at low coverages, NH_3OH^+ and NH_4^+ can be yielded, while N_2O or N_2 is the favorable product at high coverages.[19,28,29] Thus, after screening out the Co-N_4/graphene as the potential NOER catalyst candidate, we examined its interaction with NO molecules at different coverages.

At low coverage, the side-on configuration is unstable, upon full atomic relaxation, it spontaneously converts to the end-on configuration, in which the N atom

of the NO molecule is attached to the central Co atom with the distance of 1.83 Å (Fig. 2a). Meanwhile, the adsorbed NO molecule extracts 0.10 e^- from the Co-N_4 moiety, which occupies its unfilled $2\pi^*$ orbitals, thus resulting in the elongation of the N–O bond from 1.16 Å in free NO to 1.19 Å in the adsorbed NO species. The NO adsorption energy on Co-N_4/graphene is -1.48 eV, and the corresponding Gibbs free energy is -0.77 eV after taking account of the contributions from zero point energy and entropy.

To get a deeper understanding on the interaction of NO with Co-N_4/graphene, we computed the partial density of states (PDOSs) for NO adsorbed Co-N_4/graphene. As shown in Fig. 2b, there is an obvious hybridization between the N-2*p* orbitals and Co-3*d* orbitals. Especially, upon adsorption of NO molecule, the magnetic moment (0.96 μ_B) of Co-N_4/graphene disappears due to the spin-coupling interaction between Co and N atoms. In other words, there is obvious magnetic moment transfer between NO and Co-N_4/graphene. Overall, the aforementioned results showed that the NO molecule can be sufficiently activated on Co-N_4/graphene, thus facilitating the subsequent reduction reactions, and this reaction step can be written as NO(g) → NO^*. However, the direct cleavage of the activated NO on Co-N_4/graphene has to overcome an energy barrier of 4.23 eV (Fig. S1 in Supporting Information), which is even higher than that of on Pt(111) (2.30 eV),[78,79] suggesting that this reaction cannot take place at room temperature.

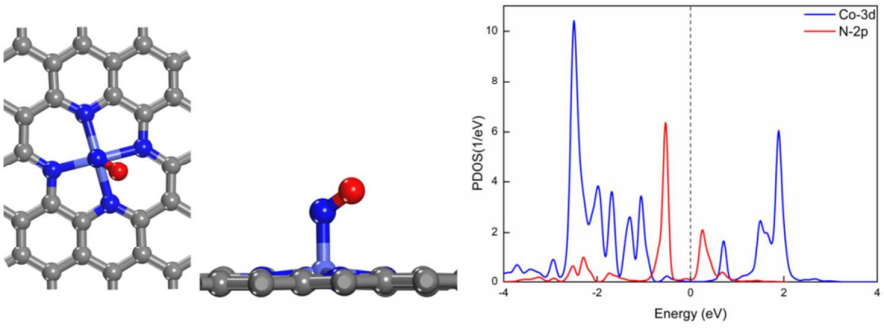

(a) (b)

Fig.2. (a) Optimized configurations and (b) Partial density of states (PDOS)of NO adsorbed on Co-N_4/graphene.

We further examined NO adsorption at higher coverage on Co-N_4/graphene by exploring the $(NO)_2$ dimer adsorption since the dimer could act as a precusor state for N_2O formation. After considering different initial configurations, three adsorbed $(NO)_2$ species were obtained (namely, D1, D2, and D3 in Fig. 3). The adsorption energies (defined as $E_{ad} = E_{(NO)2/substrate} - 2E_{NO} - E_{substrate}$) are -1.83, -1.35, and -0.96 eV for D_1, D_2, and D_3, respectively. However, after taking account of zero point energy correction and entropy effect, the ΔG values for D_1, D_2, and D_3 are −0.34, +0.14, and +0.53 eV, respectively, suggesting that only D_1 is energetically favorable. The D_1 species features a trapezoid *ONNO*-based five-membered ring, which is bound to central Co atom through its two O atoms with the Co−O bond length of 1.91 Å (Fig. 3a). As Co-N_4/graphene donates about 0.59 electrons to the adsorbed $(NO)_2$ dimer, the N-O bond length is elongated by 0.20 Å than that of isolated NO (1.16 Å). Remarkably, the D_1 species can be viewed as the interactions of two NO monomers with the central Co site via their O atoms, and this process has a small barrier of 0.28

eV (Fig. S2), indicating the kinetic feasibility of the formation of D_1 species. Note that for NO dimer adsorption, the formation of Co-O bonds (as in D_1) is more favorable, which is different from that for mono NO adsorption, in which the formation of Co-N bond is energetically preferred. The variation from the preferred Co-N adsorption for NO mononer to the preferred Co-O adsorption for NO dimer is mostly due to the unfavorable NN bond in the dimer case.

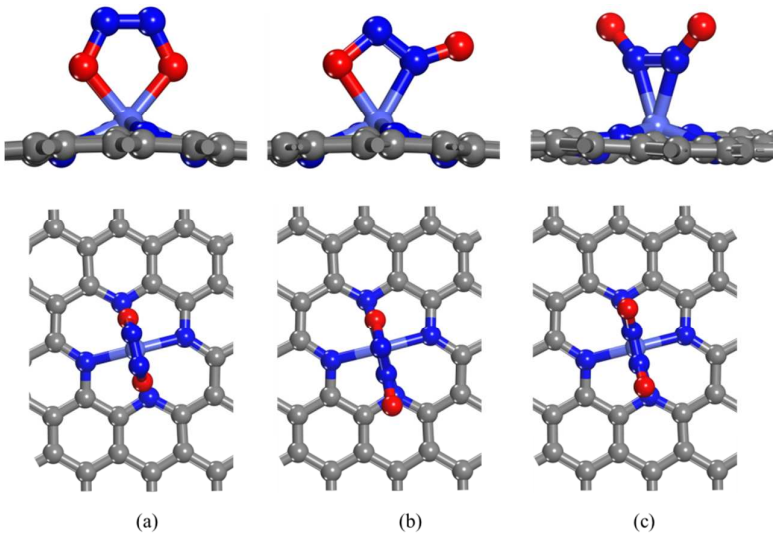

Fig. 3. Optimized configurations of $(NO)_2$ species adsorbed on Co-N_4/graphene: (a) D_1, (b) D_2, and (c) D_3.

3.3. NOER Pathways.

After confirming that NO molecule can be sufficiently activated, we explored the subsequent NOER steps on the Co-N_4/graphene, from which two possible reaction pathways were considered (Scheme 1): (I) at low coverages, the adsorbed NO molecule is reduced to NH_3/NH_4^+ through the overall reaction: NO (g) + 5 (or 6)H^+ + 5e^-→ NH_3 (or NH_4^+) + H_2O (*l*); (II) at high coverages, N_2O is produced under

continuous reduction conditions through the overall reaction: $2NO\ (g) + 2H^+ + 2e^- \rightarrow N_2O + H_2O\ (l)$.

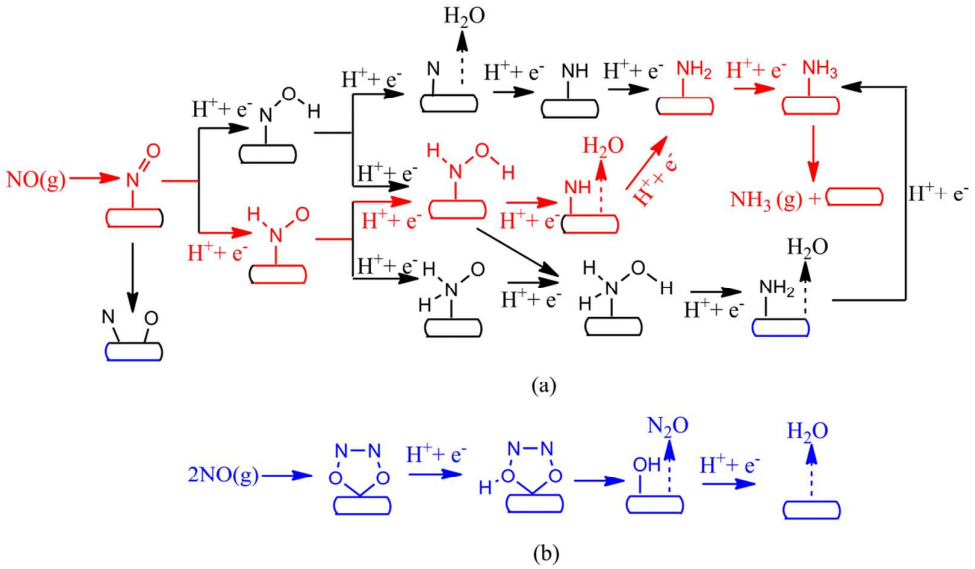

Scheme 1: Schematic depiction of the pathways of NO electrochemical reduction on the Co-N_4/graphene surface at (a) low and (b) high coverages. The preferred pathways are plotted in red (for low coverage) and blue (for high coverage) lines.

3.3.1. Ammonia Formation at Low NO Coverage. Figure 4 presents the atomic configurations of the intermediates in each elementary step of the NOER on Co-N_4/graphene at low coverage, while the corresponding free energy profiles are summarized in Fig. 5. The activated NO^* species is firstly hydrogenated by interacting with a proton coupled with an electron transfer. As both N and O atoms of the adsorbed NO are possible active sites for the adsorption of the first hydrogen, two different intermediates, HNO^* species and NOH^* species, can be formed, and the former one is thermodynamically preferred. For the HNO^* species, the newly formed N-H bond length is 1.04 Å, and the Co-N and N-O bonds are 1.86, and 1.25 Å,

respectively. For comparison, the O-H, Co-N, and N-O bond lengths in the NOH^* species 0.99, 1.82, and 1.35 Å, respectively. At zero electrode potential, the HNO^* formation step has a free energy uphill of 0.12 eV and an energy barrier of 0.70 eV, while the NOH^* formation has an unfavorable larger free energy increase (0.95 eV) but a smaller energy barrier (0.60 eV).

The thermodynamic and kinetic competition for the formation of NOH^* and HNO^*, as found above, has also been observed for NO electrochemical reduction on Pt(100). [19, 68, 69] Note that the exact mechanism of NOER to various products through HNO^* or NOH^* intermediates is still under debate. For example, Koper *et al.* proposed that ammonia is produced through the HNO species via NO → HNO → H_2NO → $NH_4^+ + H_2O$,[14, 80] while Cuesta *et al.* argued that NOH could be a favored intermediates.[25]

Which intermediate is more preferred on the Co-N_4/graphene, HNO^* or NOH^*? To address this question, we performed first principles molecular dynamics (MD) simulations using the NVT ensemble with Nosé-Hoover chain for thermostats at 300 K (please see Fig. S3 and Movie 1 for details, in which some snapshots of the intermediate configurations are inserted). The NO^* on the Co-N_4/graphene with some H atoms on the N sites around Co site was taken as the initial structure. Our MD computations showed that the NO^* species transforms into HNO^* species by interacting with an adjacent H atom at about 134 fs. Thus, the thermodynamically more favorable HNO^* intermediate can be easily formed, and the NOER on the Co-N_4/graphene catalyst is expected to go through the HNO pathway rather than the

NOH pathway.

Once formed, the HNO^* species will be further hydrogenated by reacting with another proton through two possible reaction pathways: H atom is attached at (i) the O site apart from the Co dopant to form $HNOH^*$ species and (ii) the N site bound with the Co dopant to give H_2NO^* species. Our computations showed that the Gibbs free energy of $HNOH^*$ formation is 0.27 lower than that of H_2NO^* species, thus the $HNOH^*$ formation is more favorable with a zero energy barrier. Interestingly, the subsequent addition of H atom to $HNOH^*$ or H_2NO^* species could lead to the formation of H_2NOH^* species (Scheme 1). The other possible pathway for the $HNOH^*$ species is its hydrogenation to NH^* species, and the concomitant desorption of a H_2O molecule from the catalyst surface. For these three elementary reactions, i.e., (1) $HNOH^* \rightarrow H_2NOH^*$, (2) $H_2NO^* \rightarrow H_2NOH^*$, and (3) $HNOH^* \rightarrow NH^* + H_2O$, the computed ΔG values are -0.01, +0.27, and -0.57 eV, respectively, indicating that the formation of NH^* species is more favorable thermodynamically than that of H_2NOH^* species. Remarkably, the energy barrier for $HNOH^*$ protonation to NH^* species is only 0.25 eV. The resulting NH^* species on the Co-N_4/graphene can be hydrogenated to NH_3 by reacting with another two protons coupled with electrons, and the free energies are downhill by 1.70 and 1.00 eV, respectively. Notably, we also computed the kinetics for the reductions of NH^* to NH_2^* and NH_2^* to NH_3^*, and very small barriers of 0.10 eV were observed. As the final step, the newly formed NH_3 molecule can be released from the Co-N_4/graphene by overcoming a positive ΔG value of 0.43 eV.

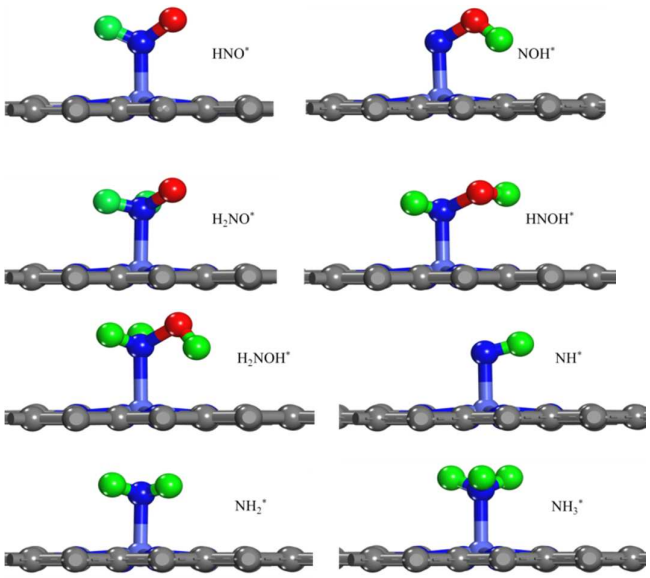

Fig. 4. The optimized geometric structures of various species (HNO^*, NOH^*, H_2NO^*, $HNOH^*$, H_2NOH^*, NH^*, NH_2^*, and NH_3^*) along the reaction path of NOER proceeded on Co-N_4/graphene at low coverages.

Overall, the NOER occurring on Co-N_4/graphene at low coverage prefers to proceed through the HNO^* and $HNOH^*$ intermediates: $NO(g) \rightarrow NO^* \rightarrow HNO^* \rightarrow HNOH^* \rightarrow NH^* \rightarrow NH_2^* \rightarrow NH_3^* \rightarrow NH_3$, in which the hydrogenation reaction of the adsorbed NO^* species to HNO^* is the potential-determining step due to its maximum Gibbs free energy (0.12 V) among all elementary steps at zero electrode potential. According to the standard onset potential method, which has been widely used to elucidate the catalytic activity of electrocatalysts for various electrocatalytic reactions, including oxygen reduction,[81] CO_2 reduction,[82] and nitrogen reduction,[48] the onset potential for NO electrochemical reduction is -0.12 V, under which the Gibbs free energies of all the reaction intermediates become downhill relative to NO^*. Especially, such an onset potential is very close to that of on Pt (111) surface (0.00 V),[19,29] and is

even lower than that on Pt(100) surface (-0.20 V).[19, 28] Thus, the Co-N_4/graphene would exhibit rather high catalytic activity toward NOER at low coverage.

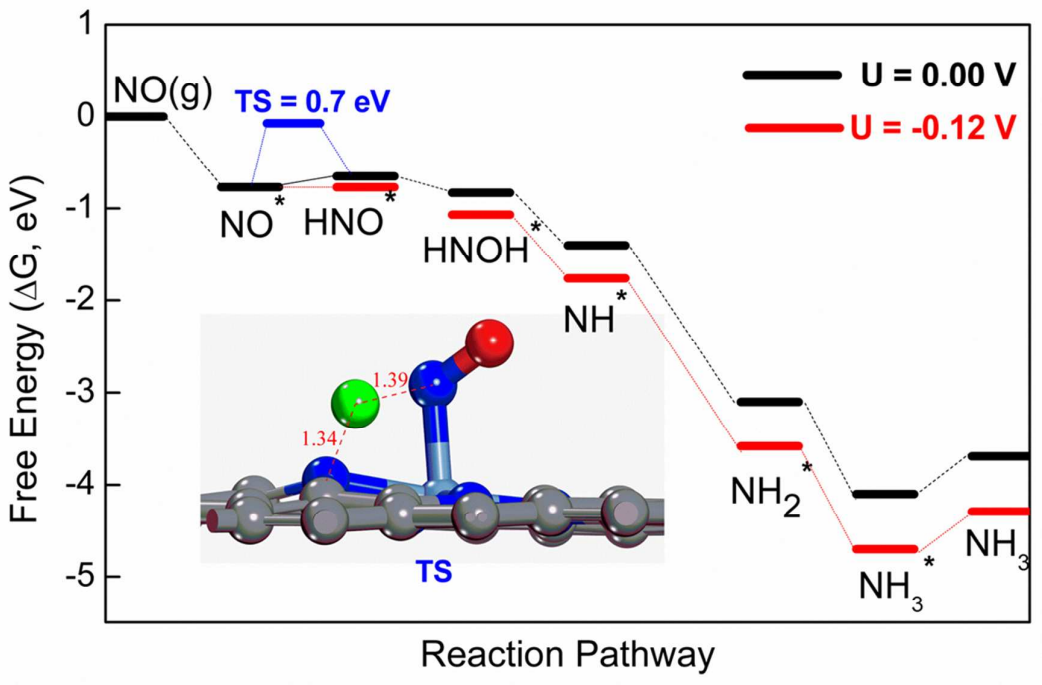

Fig. 5. Free-energy diagrams for the NOER on Co-N_4/graphene at low coverage along the most energetically favorable pathway at pH=0 and at zero or onset potential. TS is the transition state of the rate-determining step ($NO^* \rightarrow HNO^*$). The activation barriers for other steps (not shown in the figure) are 0.00, 0.25, 0.10, and 0.10 eV, respectively, for $HNO^* \rightarrow HNOH^* \rightarrow NH^* \rightarrow NH_2^* \rightarrow NH_3^*$

3.3.2. N_2O Formation at High NO Coverage. In addition to ammonia, N_2O could be yielded during NO electroreduction reaction at high coverage through the $(NO)_2$ dimer (D_1 species in Fig. 3a). Figure 6 presents the optimized atomic configurations of the key intermediates ($HONNO^*$ and OH^*) along this reaction pathway, while the corresponding free energy profiles are summarized in Fig. 7. Our

computational results showed that the D_1 intermediate can be easily hydrogenated by adsorbing a proton coupled with an electron transfer, forming an HONNO* species adsorbed on Co site (Fig. 6), in which the H atom binds to one O atom with a O-H length of 0.98 Å. This process is slightly uphill in the free energy profile by 0.11 eV (Fig. 7) and has a small energy barrier of 0.19 eV. Subsequently, the newly formed HONNO* species would dissociate into OH*, and one N_2O molecule is released from the surface of Co-N_4/graphene after overcoming a low energy barrier of 0.09 eV. Remarkably, the Gibbs free energy for this reaction step, HNOON* → OH* + N_2O, decreases by 2.64 eV. Finally, the remaining OH group on Co site reacts with one proton coupled with an electron transfer to form H_2O molecule. The ΔG value for this step is –0.75 eV, and no energy barrier is involved.

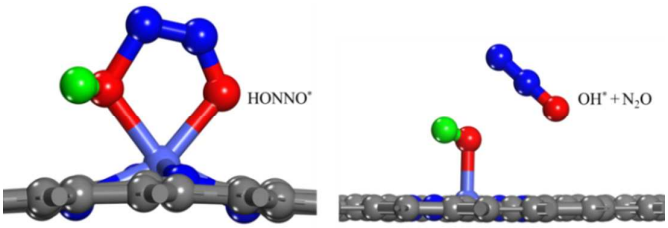

Fig. 6. The optimized geometric structures of key intermediates (HONNO* and OH*) along the reaction path of NOER proceeded on Co-N_4/graphene at high coverages.

Overall, at high coverage, NO would be reduced to N_2O through a 2e pathway, namely, 2NO(g) → $(NO)_2^*$ → HONNO*→ N_2O(g) + OH* → N_2O(g) + H_2O (l), in which the protonation of $(NO)_2$ species to HONNO* is the potential-limiting step with the maximum ΔG value (0.11 eV), thus an onset potential of -0.11 V for NOER along this pathway is obtained. Moreover, the highest energy barrier in this pathway is only

0.28 eV (for 2NO (g) → $(NO)_2^*$), which is much smaller than that in the ammonia formation pathway under low NO coverage (0.70 eV). Therefore, the NOER on Co-N_4/graphene may kinetically prefer the N_2O formation via the 2e reduction pathway rather than the NH_3 formation via the 5e reduction pathway.

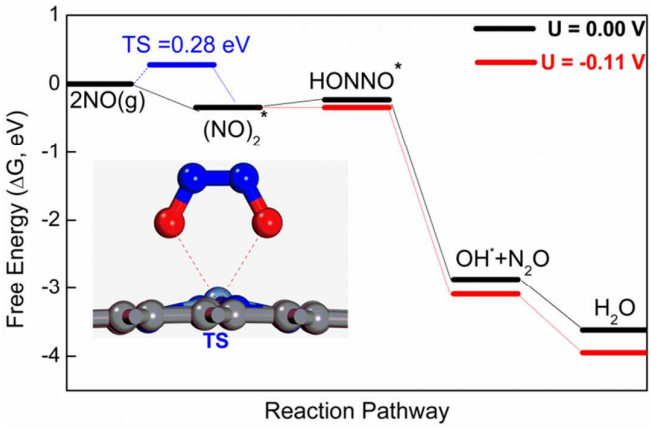

Fig. 7. Free-energy diagrams for the NOER on Co-N_4/graphene at high coverages along the most energetically favorable pathway at pH=0 and at zero or onset potential. TS is the transition state of the rate-determining step (2NO (g) → $(NO)_2^*$). The activation barriers for other steps (not shown in the figure) are 0.19, 0.09, and 0.00 eV, respectively, for $(NO)_2^*$ → HONNO* → N_2O(g) + OH* → N_2O(g) + H_2O (l).

3.4. Mechanism of High NOER Activity on the Co-N_4/Graphene Surface.

Based on the aforementioned discussions, the high catalytic activity of the Co-N_4 moiety embedded into graphene could originate from its binding strength with the intermediates of NOER, which in turn is determined by the electronic properties of catalysts. To gain deeper insight into the superior NOER catalytic activity of Co-N_4/graphene, we compared the electronic properties of these TM-N_4/graphenes according to the d-band model.[83-85] In this theory, the position of the d-band center of

the catalytic center closer to the Fermi level causes anti-bonding states to a higher energy, leading to a stronger binding strength between the catalytic center and the adsorbed NO species.

Figure 8 presents the variation of the computed ΔG values of NO adsorption on TM-N_4/graphene with the d-band centers of the central TM atoms, which demonstrates a clear linear relationship. For example, the computed d-band centers of the single Fe, Co, and Cu atoms embedded into graphene are −2.97, −3.19, and −3.52 eV, respectively, which are well consistent with their corresponding adsorption strength with NO species (ΔG = -1.27, -0.77, and +0.06 eV). In this sense, the obvious difference ΔG values of NO adsorption on various TM-N_4/graphene can be directly correlated with the shift of d-band center. The moderate d-band center on Co-N_4/graphene leads to a moderate interaction of the surface with the adsorbed NO, which is responsible for faster kinetics for the NOER on Co-N_4/graphene.

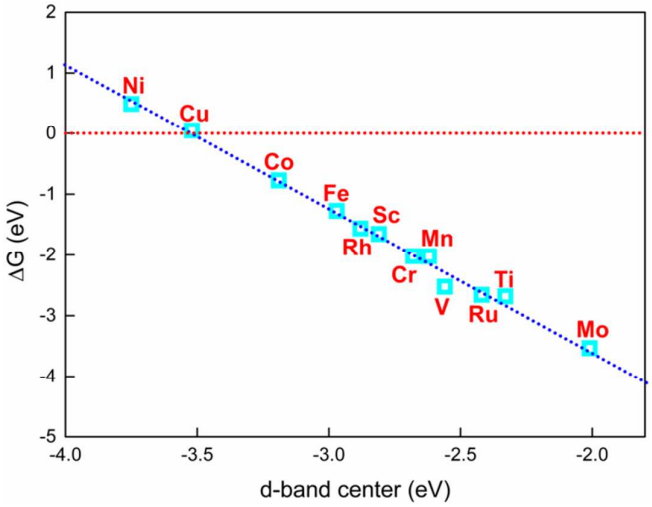

Fig. 8. Calculated NO adsorption free energies (ΔG) on TM-N_4/graphenes versus d-band center of the central TM atoms.

4. CONCLUSIONS

In summary, our DFT computations revealed that the Co-N_4 moiety embedded into graphene exhibits superior NOER catalytic activity, and ammonia can be formed through the HNO intermediate species at low coverages, while at high coverages, N_2O can be easily formed. Especially, the onset potential of NOER on Co-N_4/graphene (about -0.12 V) is comparable to (or even better than) those of Pt-based catalysts. Note that Co-N_4 moiety embedded into graphene has been successfully fabricated by various groups, and its outstanding chemical and thermal stability during electrocatalysis endows it wide applications as an efficient catalyst for oxygen reduction and evolution reaction,[86-89] hydrogen evolution reaction,[90] photocatalytic hydrogen production,[91] selective oxidation of alcohols,[92] chemoselective hydrogenation of nitroarenes,[93] and selective catalytic hydrogenation of nitroarenes.[94] In terms of the high stability and the superior catalytic performance, we strongly believe that Co-N_4/graphene will be employed by experimental peers for electrochemical reduction of NO at ambient conditions in the quite near future, which could open a new avenue of electrochemical denitrification by the single-atom electrocatalyst.

ACKNOWLEDGEMENTS

This work was financially supported in China by the Excellent Young Foundation of Harbin Normal University (Grant No. XKYQ201304), and in USA by NSF-CREST Center for Innovation, Research and Education in Environmental

Nanotechnology (CIRE2N) (Grant Number HRD-1736093) and NASA (Grant 17-EPSCoRProp-0032).

Electronic Supplementary Information

The minimum energy paths (MEP) for NO dissociation and formation of the energetically most favorable $(NO)_2$ dimer on the Co-N_4 moiety embedded into graphene; Some key snapshots during the trajectories of the first principles MD simulations of NO reduction on Co-N_4/graphene at 300 K. This material is available free of charge via the Internet at http://pubs.acs.org.

References

1. D. E. Canfield, A. N. Glazer and P. G. Falkowski, *Science* **2010,** *330*, 192-196.

2. J. N. Galloway, A. R. Townsend, J. W. Erisman, M. Bekunda, Z. Cai, J. R. Freney, L. A. Martinelli, S. P. Seitzinger and M. A. Sutton, *Science* **2008,** *320*, 889-892.

3. V. Rosca, M. Duca, M. T. de Groot and M. T. M. Koper, *Chem. Rev.* **2009,** *109*, 2209-2244.

4. M. Duca and M. T. M. Koper, *Energy & Environ. Sci.* **2012,** *5*, 9726-9742.

5. S.-E. Bae and A. A. Gewirth, *Faraday Discuss.* **2009,** *140*, 113-123.

6. E. B. Molodkina, M. R. Ehrenburg, Y. M. Polukarov, A. I. Danilov, J. Souza-Garcia and J. M. Feliu, *Electrochimica Acta* **2010,** *56*, 154-165.

7. C. Roy, J. Deschamps, M. H. Martin, E. Bertin, D. Reyter, S. Garbarino, L. Roué and D. Guay, *Appl. Cata. B: Environ.* **2016,** *187*, 399-407.

8. E. Pérez-Gallent, M. C. Figueiredo, I. Katsounaros and M. T. M. Koper,

Electrochimica Acta **2017,** *227*, 77-84.

9. S.-E. Bae, K. L. Stewart and A. A. Gewirth, *J. Am. Chem. Soc.* **2007,** *129*, 10171-10180.

10. M. T. de Groot, M. Merkx and M. T. M. Koper, *J. Am. Chem. Soc.* **2005,** *127*, 16224-16232.

11. M. T. de Groot, M. Merkx, A. H. Wonders and M. T. M. Koper, *J. Am. Chem. Soc.* **2005,** *127*, 7579-7586.

12. M. Duca, M. O. Cucarella, P. Rodriguez and M. T. M. Koper, *J. Am. Chem. Soc.* **2010,** *132*, 18042-18044.

13. T. Chen, H. Li, H. Ma and M. T. M. Koper, *Langmuir* **2015,** *31*, 3277-3281.

14. M. Duca, M. C. Figueiredo, V. Climent, P. Rodriguez, J. M. Feliu and M. T. M. Koper, *J. Am. Chem. Soc.* **2011,** *133*, 10928-10939.

15. M. Duca, S. Khamseh, S. C. S. Lai and M. T. M. Koper, *Langmuir* **2010,** *26*, 12418-12424.

16. V. Rosca, G. L. Beltramo and M. T. M. Koper, *Langmuir*, 2005, 21, 1448-1456.

17. V. Rosca and M. T. M. Koper, *J. Phys. Chem. B* **2005,** *109*, 16750-16759.

18. J. Shen, Y. Y. Birdja and M. T. M. Koper, *Langmuir*, 2015, 31, 8495-8501.

19. I. Katsounaros, M. C. Figueiredo, X. Chen, F. Calle-Vallejo and M. T. M. Koper, *ACS Catal.* **2017,** *7*, 4660-4667.

20. M. T. de Groot and M. T. M. Koper, *J. Electroanal. Chem.* **2004,** *562*, 81-94.

21. M. C. Figueiredo, J. Solla-Gullón, F. J. Vidal-Iglesias, V. Climent and J. M. Feliu, *Catal. Today* **2013,** *202*, 2-11.

22. Q. Guo, T. Sun, Y. Wang, Y. He and J. Jia, *Environmental Science & Technology* **2013,** *47*, 9514-9522.

23. T.-J. Huang, C.-Y. Wu and Y.-H. Lin, *Environ. Sci. & Technology* **2011,** *45*, 5683-5688.

24. T.-J. Huang, D.-Y. Chiang, C. Shih, C.-C. Lee, C.-W. Mao and B.-C. Wang, *Environ. Sci. & Technology* **2015,** *49*, 3711-3717.

25. T.-J. Huang, S.-H. Hsu and C.-Y. Wu, *Environ. Sci. & Technology* **2012,** *46*, 2324-2329.

26. W. Teng, N. Bai, Y. Liu, J. Fan, and W. Zhang, *Environ. Sci. & Technology* **2018,** *52*, 230-236.

27. Y.-P. Chen, S.-Y. Liu, F. Fang, S.-H. Li, G. Liu, Y.-C. Tian, Y. Xiong and H.-Q., Yu, *Environ. Sci. & Technology* **2008,** *42*, 8465-8470.

28. A. C. A. de Vooys, M. T. M. Koper, R. A. van Santen and J. A. R. van Veen, *Electrochimica Acta*, 2001, 46, 923-930.

29. A. C. A. de Vooys, M. T. M. Koper, R. A. van Santen and J. A. R. van Veen, *J. Catal.* **2001,** *202*, 387-394.

30. A. C. A. de Vooys, G. L. Beltramo, B. van Riet, J. A. R. van Veen and M. T. M. Koper, *Electrochimica Acta*, 2004, 49, 1307-1314.

31. A. Cuesta and M. Escudero, *Phys. Chem. Chem. Phys.* **2008,** *10*, 3628-3634.

32. J. Yang, P. Sebastian, M. Duca, T. Hoogenboom and M. T. M. Koper, *Chem. Commun.* **2014,** *50*, 2148-2151.

33. M. Duca, V. Kavvadia, P. Rodriguez, S. C. S. Lai, T. Hoogenboom and M. T. M.

Koper, *J. Electroanal. Chem.* **2010,** *649*, 59-68.

34. H. J. Chun, V. Apaja, A. Clayborne, K. Honkala and J. Greeley, *ACS Catal.* **2017,** *7*, 3869-3882.

35. A. Clayborne, H. J. Chun, R. B. Rankin and J. Greeley, *Angew. Chem. Intern. Ed.* **2015,** *54*, 8255-8258.

36. D. A. Finkelstein, E. Bertin, S. Garbarino and D. Guay, *J. Phys. Chem. C* **2015,** *119*, 9860-9878.

37. M. Kato, M. Okui, S. Taguchi and I. Yagi, *J. Electroanal. Chem.* **2017,** *800*, 46-53.

38. Q. F. Wang, X. B. Zhao, J. F. Zhang and X. W. Zhang, *J. Electroanal. Chem.* **2015,** *755*, 210-214.

39. R. Kamai, S. Nakanishi, K. Hashimoto and K. Kamiya, *J. Electroanaly. Chem.* **2017,** *800*, 54-59.

40. F. R. Rima, K. Nakata, K. Shimazu and M. Osawa, *J. Phys. Chem. C* **2010,** *114*, 6011-6018.

41. E. C. Tyo and S. Vajda, *Nature Nanotech.* **2015,** *10*, 577-588.

42. Q. Wu, S. Xiong, P. Shen, S. Zhao, Y. Li, D. Su and A. Orlov, *Catal. Sci. & Techn.* **2015,** *5*, 2059-2064.

43. L. Xie, P. Brault, C. Coutanceau, J.-M. Bauchire, A. Caillard, S. Baranton, J. Berndt and E. C. Neyts, *Appl. Catal. B-Environ.* **2015,** *162*, 21-26.

44. J. Liu, M. Jiao, L. Lu, H. M. Barkholtz, Y. Li, Y. Wang, L. Jiang, Z. Wu, D.-j. Liu, L. Zhuang, C. Ma, J. Zeng, B. Zhang, D. Su, P. Song, W. Xing, W. Xu, Y. Wang, Z.

Jiang and G. Sun, *Nature Commun.* **2017,** *8*, 15938.

45. X. F. Yang, A. Q. Wang, B. T. Qiao, J. Li, J. Y. Liu and T. Zhang, *Acc. Chem. Res.* **2013,** *46*, 1740-1748.

46. J. Kim, H.-E. Kim and H. Lee, *ChemSusChem*, 2017, *DOI: 10.1002/cssc.201701306.*

47. C. Zhu, S. Fu, Q. Shi, D. Du and Y. Lin, *Angew. Chem. Intern. Ed.* **2017,** *56*, 13944-13960.

48. J. Zhao and Z. Chen, *J. Am. Chem. Soc.* **2017,** *139*, 12480-12487.

49. J. Deng, H. Li, J. Xiao, Y. Tu, D. Deng, H. Yang, H. Tian, J. Li, P. Ren and X. Bao, *Energy & Environ. Sci.* **2015,** *8*, 1594-1601.

50. J. Liu, B. R. Bunes, L. Zang and C. Wang, *Environ. Chem. Lett.* **2017**, *https://doi.org/10.1007/s10311-017-0679-2*.

51. J. Wang, H. Zhang, and X. Wang, *Small Methods* **2017,** *1*, (6), 1700118.

52. S.Yang, J. Kim, Y. J. Tak, A. Soon and H. Lee, *Angew. Chem. Intern. Ed.* **2016,** *55*, 2058-2062.

53. J. Gao, N. Ma, J. Zhai, T. Li, W. Qin, T. Zhang and Z. Yin, *Industrial & Engin. Chem. Res.* **2015,** *54*, 7984-7989.

54. Y. Qian, Z. Liu, H. Zhang, P. Wu and C. Cai, *ACS Appl. Mater. & Inter.* **2016,** *8*, 32875-32886.

55. E. C. M. Tse, J. A. Varnell, T. T. H. Hoang and A. A. Gewirth, *J. Phys. Chem. Lett.* **2016,** *7*, 3542-3547.

56. L. Lin, Q. Zhu and A.-W. Xu, *J. Am. Chem. Soc.* **2014,** *136*, 11027-11033.

57. W. Ju, A. Bagger, G.-P. Hao, A. S. Varela, I. Sinev, V. Bon, B. Roldan Cuenya, S. Kaskel, J. Rossmeisl and P. Strasser, *Nature Commun.* **2017,** *8*, 944.

58. J. T. Feaster, C. Shi, E. R. Cave, T. Hatsukade, D. N. Abram, K. P. Kuhl, C. Hahn, J. K. Nørskov and T. F. Jaramillo, *ACS Catal.* **2017,** *7*, 4822-4827.

59. C. Zhao, X. Dai, T. Yao, W. Chen, X. Wang, J. Wang, J. Yang, S. Wei, Y. Wu and Y. Li, *J. Am. Chem. Soc.* **2017,** *139*, (24), 8078-8081.

60. X.-F. Li, Q.-K. Li, J. Cheng, L. Liu, Q. Yan, Y. Wu, X.-H. Zhang, Z.-Y. Wang, Q. Qiu and Y. Luo, *J. Am. Chem. Soc.* **2016,** *138*, 8706-8709.

61. H. Fei, J. Dong, M. J. Arellano-Jiménez, G. Ye, N. Dong Kim, E. L. G. Samuel, Z. Peng, Z. Zhu, F. Qin, J. Bao, M. J. Yacaman, P. M. Ajayan, D. Chen and J. M. Tour, *Nature Commun.* **2015,** *6*, 8668.

62. B. Delley, *J. Chem. Phys.* **1990,** *92*, 508-517.

63. B. Delley, *J. Chem. Phys.* **2000,** *113*, 7756-7764.

64. J. P. Perdew, K. Burke and M. Ernzerhof, *Phys. Rev. Lett.* **1996,** *77*, 3865-3868.

65. S. Grimme, *J. Comput. Chem.* **2006,** *27*, 1787-1799.

66. B. Delley, *Phys. Rev. B* **2002,** *66*, 155125.

67. P. Liu and J. A. Rodriguez, *J. Am. Chem. Soc.* **2005,** *127*, 14871-14878.

68. N. Govind, M. Petersen, G. Fitzgerald, D. King-Smith and J. Andzelm, *Comput. Mater. Sci.* **2003,** *28*, 250-258.

69. F. L. Hirshfeld, *Theoretica Chim. Acta* **1977,** *44*, 129-138.

70. J. K. Nørskov, J. Rossmeisl, A. Logadottir, L. Lindqvist, J. R. Kitchin, T. Bligaard and H. Jónsson, *J. Phys. Chem. B* **2004,** *108*, 17886-17892.

71. J. Rossmeisl, A. Logadottir and J. K. Nørskov, *Chem. Phys.* **2005,** *319*, 178-184.

72. A. A. Peterson, F. Abild-Pedersen, F. Studt, J. Rossmeisl and J. K. Nørskov, *Energy & Environ. Sci.* **2010,** *3*, 1311-1315.

73. E. Skulason, T. Bligaard, S. Gudmundsdottir, F. Studt, J. Rossmeisl, F. Abild-Pedersen, T. Vegge, H. Jonsson and J. K. Nørskov, *Phys. Chem. Chem. Phys.* **2012,** *14*, 1235-1245.

74. J. G. Howalt and T. Vegge, *Phys. Chem. Chem. Phys.* **2013,** *15*, 20957-20965.

75. J. G. Howalt, T. Bligaard, J. Rossmeisl and T. Vegge, *Phys. Chem. Chem. Phys.* **2013,** *15*, 7785-7795.

76. A. Klamt and G. Schuurmann, *J. Chem. Soc., Perkin Tran.* **1993**, *2,* 799-805.

77. G. Rothenberg, *Catalysis:Concepts and Green Applications.* Wiley-VCH. 2008, **2008**, *p65*, ISBN 3-527-31824-0.

78. Z.-H. Zeng, J. L. F. Da Silva, H.-Q. Deng and W.-X. Li, *Phys. Rev. B* **2009,** *79*, 205413

79. C. A. Farberow, J. A. Dumesic and M. Mavrikakis, *ACS Catal.* **2014,** *4*, 3307-3319.

80. J. Yang, F. Calle-Vallejo, M. Duca and M. T. M. Koper, *ChemCatChem* **2013,** *5*, 1773-1783.

81. Y. Wang, H. Yuan, Y. Li, Y. and Z. Chen, *Nanoscale* **2015,** *7*, 11633-11641.

82. Z. Wang, J. Zhao and Q. Cai, *Phys. Chem. Chem. Phys.* **2017,** *19*, 23113-23121.

83. B. Hammer and J. K. Nørskov, *Nature* **1995,** *376*, 238-240.

84. B. Hammer and J. K. Nørskov, In *Adv. Catal.*, Academic Press: 2000; Vol. 45, pp

71-129.

85. Greeley Jeff, J. K. Nørskov, M. Mavrikakis, *Annual Rev. Phys. Chem.* **2002,** *53*, 319-348.

86. P. Yin, T. Yao, Y. Wu, L. Zheng, Y. Lin, W. Liu, H. Ju, J. Zhu, X. Hong, Z. Deng, G. Zhou, S. Wei and Y. Li, *Angew. Chem. Intern. Ed.* **2016,** *55*, 10800-10805.

87. X. Qiao, S. Liao, R. Zheng, Y. Deng, H. Song, and L. Du, *ACS Sustainable Chem. & Engin.* **2016,** *4*, 4131-4136.

88. A. Zitolo, N. Ranjbar-Sahraie, T. Mineva, J. Li, Q. Jia, S. Stamatin, G. F. Harrington, S. M. Lyth, P. Krtil, S. Mukerjee, E. Fonda and F. Jaouen, *Nature Commun.* **2017,** *8*, 957.

89. T. He, H. Xue, X. Wang, S. He, Y. Lei, Y. Zhang, R. Shen, Y. Zhang and J. Xiang, *Nanoscale* **2017,** *9*, 8341-8348.

90. L. Zhang, W. Liu, Y. Dou, Z. Du and M. Shao, *J. Phys. Chem. C* **2016,** *120*, 29047-29053.

91. Q. Zhao, W. Yao, C. Huang, Q. Wu and Q. Xu, *ACS Appl. Mater. & Inte.* **2017,** *9*, 42734-42741.

92. M. Li, S. Wu, X. Yang, J. Hu, L. Peng, L. Bai, Q. Huo and J. Guan, *Appl. Catal. A: General* **2017,** *543*, 61-66.

93. W. Liu, L. Zhang, W. Yan, X. Liu, X. Yang, S. Miao, W. Wang, A. Wang and T. Zhang, *Chem. Sci.* **2016,** *7*, 5758-5764.

94. X. Sun, A. I.Olivos-Suarez, D. Osadchii, M. J. V. Romero, F. Kapteijn and J. Gascon, *J. Catal.* **2018,** *357*, 20-28.

TOC